Tellus (1977), *29*, 523–529

Hemispheric asymmetry of oceanic heat budget in the Equatorial Atlantic and Eastern Pacific

By STEFAN HASTENRATH, *Department of Meteorology, The University of Wisconsin, Meteorology and Space Science Building, 1225 West Dayton Street, Madison, Wisconsin, 53706, U.S.A.*

(Manuscript received September 2, 1976; in final form May 31, 1977)

ABSTRACT

The oceanic heat budget is studied on the basis of ship observations during 1911–70 compiled by one degree square areas. The clockwise turning cross-equatorial surface air flow is conducive to upwelling to the South and downwelling to the North of the Eastern Pacific and Atlantic Equator, particularly during Northern summer. The wind-induced vertical motion field is considered a factor in maintaining the cold water tongues immediately to the South, and the strong temperature increase northward across the Equator. Net radiation is only slightly higher in the Southern hemisphere equatorial zone, but sensible and latent heat flux are greatly reduced in the cold water regions, especially in Northern summer. As a result, the ocean exports heat at the rate of 53 and 62 W m^{-2} to the South of the Atlantic and Pacific Equator, respectively, compared to an export of only 29 and an import of 3 W m^{-2} in the Northern hemisphere equatorial zone.

1. Introduction

The vast tropical seas have traditionally been thought of as horizontally uniform in thermal pattern and hydrospheric heat budget. The coarse spatial resolution of earlier maps (Budyko, 1963) conveys this notion for the equatorial belt in particular. Long-term ship observations in the tropical Atlantic and Eastern Pacific permitted an analysis of key meteorological elements and of the oceanic energy budget in considerable detail. Some implications for the heat budget of the equatorial oceans are discussed in the present paper.

2. Data

Ship observations taken over the tropical Atlantic and Eastern Pacific during 1911–70 were obtained from the National Climatic Center at Asheville, North Carolina, and compiled into a climatic atlas (Hastenrath & Lamb, 1977), with data being processed by one degree square areas. An atlas of the oceanic heat budget is in preparation. Some 3.5 million ship observations are available for the ocean areas depicted in Figs. 1–8.

3. Surface wind field and sea temperature

Fig. 1 depicts the lower tropospheric flow at the height of the Northern summer by way of example. For a complete ensemble of monthly charts of key observed elements and derived quantities, reference is made to the atlas (Hastenrath & Lamb, 1977). Over both the Eastern Pacific and Atlantic, the Southern hemisphere trades cross the Equator, recurve to Southwesterly, and meet the Northeast trades along an extended discontinuity in the Northern hemisphere. The discontinuity reaches its northernmost position in Northern summer, and recedes equatorward towards winter. Of importance in the following, negative vorticity occupies a broad band extending to either side of the Equator. The curl of the wind stress has a similar pattern.

Various mechanisms may cooperate in maintaining the sea surface temperature pattern depicted in Fig. 1. This is characterized by a band of cold water to the South of the Eastern Atlantic and Pacific Equator, and steep meridional temperature gradient across the Equator into the Northern hemisphere. First, lateral advection may be a factor both in the downstream portion of the Canary Current and in the cold water region of the Southeastern Equatorial Atlantic. Further, wind-induced

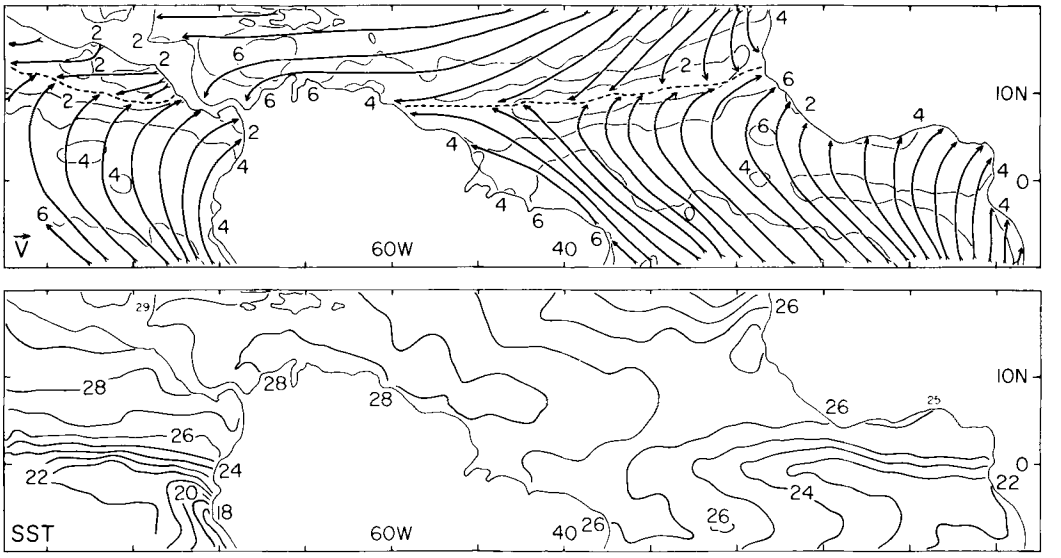

Fig. 1. July/August. Top, surface wind field, isotachs in m s^{-1}; bottom, sea surface temperature, in degrees C.

large-scale upwelling may play a role in the cold tongue immediately to the South of the Equator. Two separate mechanisms are considered in the following.

For steady-state ocean conditions away from the immediate vicinity of coasts and the Equator, vertical motion near the bottom of the mixed layer can be estimated from (Yoshida & Mao, 1957):

$$w = \frac{1}{\rho f}\left(\frac{\partial \tau_y}{\partial x} - \frac{\partial \tau_x}{\partial y}\right) \qquad (1)$$

Following conventional notation, ρ denotes density (of sea water), f Coriolis parameter and τ_x and τ_y are the zonal and meridional components of surface wind stress $\vec{\tau}$. It is noted that negative wind stress curl calls for upwelling in the Southern and for downwelling in the Northern hemisphere with largest values near the Equator, shear terms neglected in the derivation of eq. (1) conceivably accounting for continuity. For computational details reference is made to the atlas.

A third mechanism, also involving wind-induced vertical motion in the ocean, has been discussed in qualitative terms by Cromwell (1953). He showed that oceanic Ekman transport associated with Southeasterly wind could result in divergence and upwelling in a band extending from the Southern hemisphere to North of the Equator, and an oceanic convergence band at some low latitude in the Northern hemisphere. This mechanism is interesting in relation to the SST pattern in Fig. 1, which shows the strongest meridional variation North of rather than across the Equator.

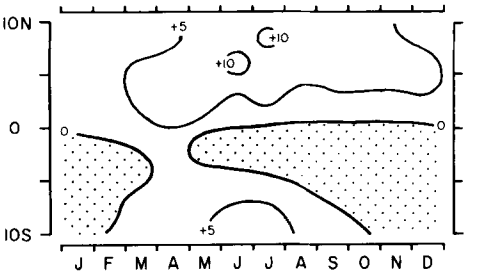

Fig. 2. Eastern Atlantic latitudinal and seasonal variation of temperature difference sea minus air at 10–30 W, in tenths of degrees C, with dot roster denoting negative areas.

The observed SST pattern, Fig. 1, may result from some combination of the mechanisms reviewed above. The SST pattern in turn is expected to be relevant for processes in the lower atmosphere.

The cold water tongues to the South of the Equator are best developed in Northern summer. The plots of temperature contrasts at the interface between ocean and atmosphere in Figs. 2 and 3 further illustrate the large latitudinal and seasonal variations of the thermal pattern in the equatorial

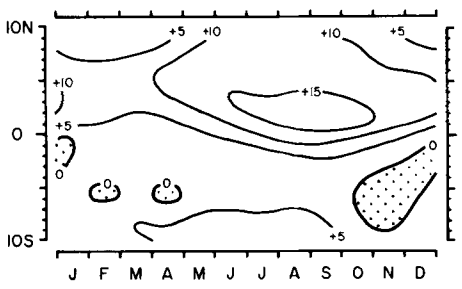

Fig. 3. Eastern Pacific latitudinal and seasonal variation of temperature difference sea minus air at 80–100 W. Symbols as in Fig. 2.

region. These have previously been discussed by Flohn (1972). The field of sea-air temperature difference is decisive for the hemispheric asymmetry of the oceanic heat budget.

4. Basic theory of oceanic heat budget

The heat budget equation for the oceanic water body can in approximate form be written:

$$SW\uparrow\downarrow + LW\uparrow\downarrow = Q_s + Q_e + (Q_v + Q_t) \qquad (2)$$

The left-hand terms are net shortwave and longwave radiation at the ocean surface, and the right-hand terms denote sensible and latent heat flux at the sea-air interface, heat export and storage within the ocean, respectively.

For the computation of net shortwave radiation $SW\uparrow\downarrow$ a variety of empirical formulae has been suggested (e.g. Budyko, 1958), using total cloudiness C_T and latitude as input. In the present study use was made of the theoretical framework presented by Bernhardt & Philipps (1958). Preference was given to Bernhardt & Philipps' (1958) over Budyko's (1958) method, because it allows for spatial variation of water vapor turbidity and would account for varying dust turbidity as pertinent information may become available. For comparison both procedures were applied to actual data, with the following results. Global radiation at cloudless sky computed from the Bernhardt and Philipps method is by about 15 W m^{-2} smaller than Budyko's latitude-mean tabulation. However, variations along a latitude circle resulting from the humidity pattern are of the same magnitude, but are ignored by the Budyko procedure. For global radiation at actual cloud cover, Bernhardt and Philipps' method yields values only about 5–10 W m^{-2}, or a few percent, smaller than Budyko's procedure: Budyko uses a somewhat stronger reduction of radiation due to cloudiness. Both methods assume the same value for the albedo of the ocean surface. Consequently maps of net shortwave radiation at actual cloud cover differ by a few percent. This is well within the uncertainty of either method.

Net longwave radiation was computed from Brunt's formula (Budyko, 1958)

$$LW\uparrow\downarrow = \varepsilon\sigma T_w^4(0.39-0.056\sqrt{q})(1-0.53C_T^2) + 4\varepsilon\sigma T_w^3(T_w - T_a) \qquad (3)$$

sea surface temperature T_w and air temperature T_a being in degrees K, and surface specific humidity q in gm/kg, emissivity $\varepsilon = 1$ and Stefan-Boltzmann's constant $\sigma = 567 \times 10^{-10}$ W m^{-2} K^{-4}.

Sensible and latent heat flux were calculated from the bulk-aerodynamic equations:

$$Q_s = \rho C_D c_p (T_w - T_a)V \qquad (4)$$

$$Q_e = \rho C_D L(q_w - q_a)V \qquad (5)$$

Values of $\rho = 1.175$ kg m^{-3} and $C_D = 1.4 \times 10^{-3}$ were used for air density and drag coefficient, respectively. c_p is specific heat at constant pressure and L latent heat of evaporation. The saturation specific humidity corresponding to the sea surface temperature T_w was computed for q_w, with reference to a salinity of 35 per mille; and scalar mean wind speed was used for V.

Of the observational data mentioned in Section 2, the following elements thus served as input to the heat budget calculations: total cloudiness, dew point, and pressure, for $SW\uparrow\downarrow$; sea surface and air temperature, dew point, pressure and cloudiness for $LW\uparrow\downarrow$; sea surface and air temperature, dew point, pressure, and scalar wind speed for Q_s and Q_e.

Time-averaged data were used in the present calculations. Covariance between elements can make the product of averages differ from the average of products, and C_D depends on stability (Bunker, 1976; Bunker & Worthington, 1976). However, these effects may be of subordinate importance for the low-latitude oceans mapped here. In fact, Bunker's (1976) annual maps of Q_e and Q_s for the North Atlantic are rather similar to the present charts: only in limited areas are his figures of Q_e by about 15 W m^{-2} larger than the

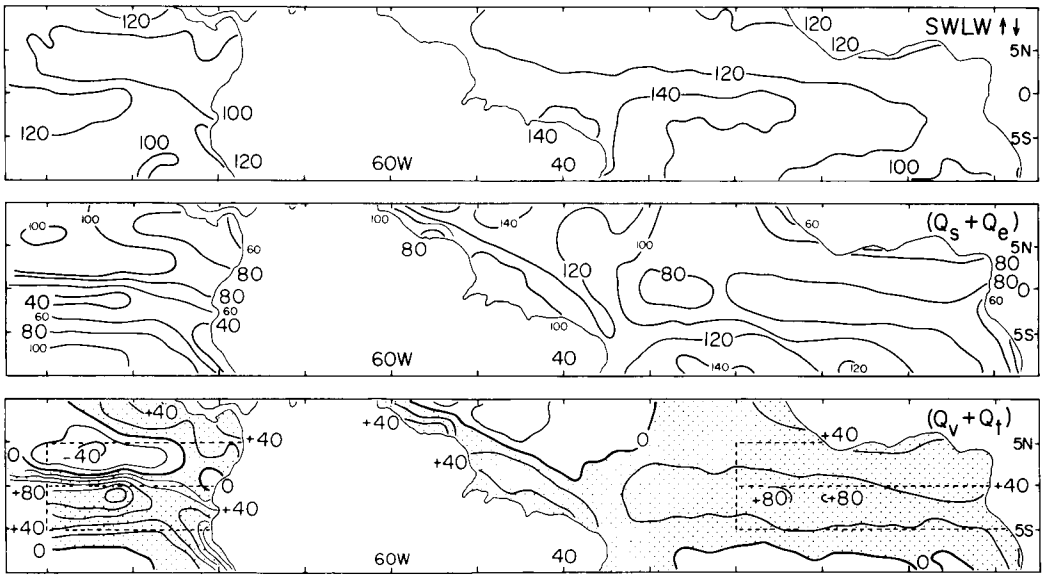

Fig. 4. Annual mean maps of oceanic heat budget. Top, net radiation SWLW↑↓; middle, sum of sensible and latent heat flux ($Q_s + Q_e$); bottom, residual divergence of heat transport and storage within the oceanic water body ($Q_v + Q_t$), with dot roster denoting export; all in W m^{-2}. Broken line rectangles indicate areas referred to in Figs. 5–8, respectively.

present ones, a difference of about 10 percent. However, Bunker's (1976) values of net radiation SWLW↑↓, calculated from somewhat different empirical formulae, are systematically larger than in Fig. 1. Consequently, his residual ($Q_v + Q_t$) differs from Fig. 4 towards larger positive values. Within the error limits of calculation methods this may be accounted for by a smaller emissivity and somewhat different coefficients in the various equations. The coarse grid of Budyko's (1963) charts, as discussed by Bunker & Worthington (1976), precludes a meaningful comparison of spatial patterns. In the present study, annual maps of heat budget components were constructed from the sets of twelve monthly computations. All maps were machine-isoplethed and then re-drawn by hand.

5. Spatial pattern

Fig. 4 maps the annual mean of oceanic heat budget components. Net radiation SWLW↑↓ largely reflects the distribution of cloudiness apart from the broad latitudinal control. Spatial variations are relatively modest with smallest values in the zonally oriented bands of abundant cloud cover in the Northern hemisphere, and larger radiative heat gain in the regions of scarce cloudiness immediately to the South of the Equator.

Sensible heat transfer is small over much of the tropical oceans, and only the sum of sensible and latent heat flux ($Q_s + Q_e$) is shown in Fig. 4. Large amounts are found in the bands of high sea temperature in the Northern hemisphere, whereas the cold water tongues immediately to the South of the Equator stand out as regions of reduced sensible and latent heat transfer.

The sum of divergence of heat transport and storage within the oceanic water body ($Q_v + Q_t$), according to eq. (2), is obtained as a residual from budget components just discussed. For the year as a whole, the residual essentially represents Q_v. The hemispheric asymmetry in the residual ($Q_v + Q_t$) is conspicuous: the cold water tongues with reduced sea-air heat exchange to the South of the Equator are powerful export regions; by contrast, greatly reduced oceanic export or even import of heat is indicated for the zone to the North of the Equator.

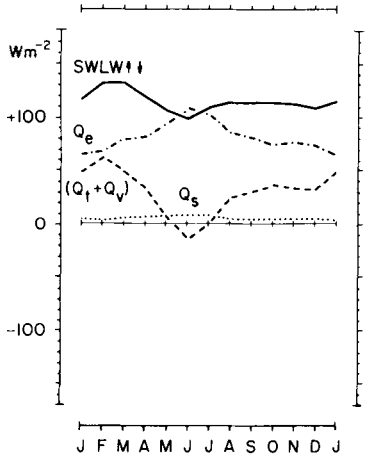

Fig. 5. Seasonal march of heat budget components in the Eastern Atlantic North of the Equator. Net radiation SWLW↑↓ solid, sensible heat flux Q_s dotted, latent heat flux Q_e dash-dotted, and residual divergence of heat transport and storage within the oceanic water body $(Q_v + Q_t)$ broken line.

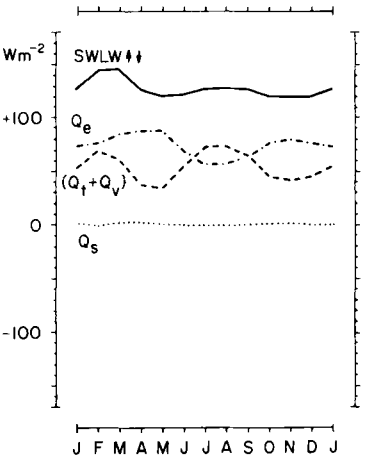

Fig. 6. Seasonal march of heat budget components in the Eastern Atlantic South of the Equator. Symbols as in Fig. 5.

6. Seasonal march

Figs. 5–6 and 7–8 compare the seasonal march of oceanic heat budget components to the North and South of the Atlantic and Pacific Equator, respectively.

As a reflection of the cloud pattern, net radiation is larger in the strips to the South, Figs. 6 and 8, than to the North of the Equator, Figs. 5 and 7.

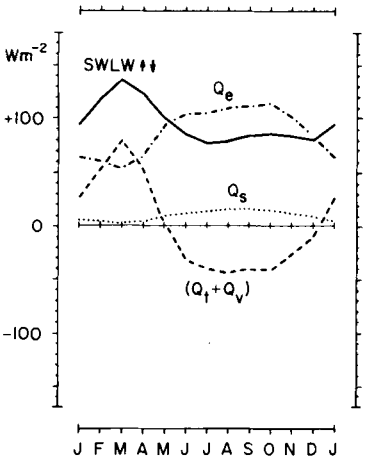

Fig. 7. Seasonal march of heat budget components in the Eastern Pacific North of the Equator. Symbols as in Figs. 5 and 6.

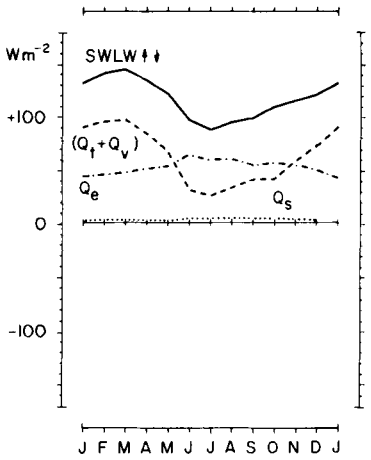

Fig. 8. Seasonal march of heat budget components in the Eastern Pacific South of the Equator. Symbols as in Figs. 5–7.

Furthermore, it is larger in the Atlantic than in the Pacific blocks. The annual range is small in all four areas. However, there are conspicuous inter-hemispheric contrasts in the latent and sensible heat flux and hence the residual heat storage and export. In the Northern hemispheric areas, Figs. 5 and 7, the maximum of latent heat flux occurs in Northern summer with high wind speed and large sea-air temperature difference, and the minimum in winter when the opposite environmental conditions prevail. Sensible heat flux is small, and directed upward throughout the year. In the regions to the

South of the Equator, Figs. 6 and 8, latent and sensible heat flux for the year as a whole are drastically reduced as a direct result of the low sea temperatures. Comparatively small values are found during Southern summer. Particularly conspicuous, however, is the broad main minimum of evaporation around the middle of the Northern summer to the South of the Atlantic Equator, Fig. 6, paralleled by a weak downward directed sensible heat flux. Over the Equatorial Eastern Pacific, Fig. 8, where seasonal variations of sea temperature are less pronounced, evaporation during Southern winter is not much higher than in summer, although a broad minimum as in Fig. 6 does not develop. The cold water tongues to the South (Figs. 6 and 8) and the regions of higher sea temperature to the North (Figs. 5 and 7) of the Atlantic and Pacific Equator further stand out in the residual heat storage and export, essentially as a result of the evaporation pattern. For the year as a whole, the cold water regions, Figs. 6 and 8, are strong exporters of heat. By comparison, the energy surplus is more moderate to the North of the Atlantic Equator, Fig. 5, and essentially nil in the area represented in Fig. 7. At the height of the Northern summer in particular, the contrast between heat excess to the South and deficit to the North of the Equator becomes most conspicuous.

7. Concluding remarks

Positive and negative areas of residual ($Q_v + Q_l$) can be partly related to major surface currents. Thus, the extensions of the cold Benguela and Humboldt Current systems would contribute in the right sense to maintain low sea surface temperatures and small sea-air temperature differences to the South of the Eastern Atlantic and Eastern Pacific Equator. However, Bunker & Worthington (1976) and Emery (1976) have given examples for large regional heat export/import to take place by mechanisms other than organized surface currents.

The long-term ship observations that have recently become available warrant an unprecedented spatial resolution in the analysis of atmospheric and hydrospheric fields. Cold water tongues immediately to the South of the Eastern Pacific and Atlantic Equator stand out sharply against high sea surface temperature and sea-air interface contrasts in the Northern hemisphere equatorial zone, especially during Northern summer. As a consequence of the thermal pattern, sensible and latent heat flux is reduced in the cold water band to the South of the Equator and remarkably so in Northern summer. For the year as a whole, this leaves an annual surplus of 62 and 53 W m^{-2} to the South of the Eastern Pacific and Atlantic Equator, contrasting with an oceanic import of 3 and an export of only 29 W m^{-2} in the corresponding blocks to the North of the Equator. Hemispheric asymmetry in the oceanic heat budget vanishes towards the Western part of the oceans.

8. Acknowledgements

This study was supported by the Office for Climate Dynamics of the National Science Foundation. P. Lamb and P. Guetter did the computer programming.

REFERENCES

Bernhardt, F. & Philipps, H. 1958. Die räumliche und zeitliche Verteilung der Einstrahlung, der Ausstrahlung, und der Strahlungsbilanz im Meeresniveau, I. Die Einstrahlung. *Abh. Meteorol. Hydrol. Dienst. DDR, 45,* Akademie-Verlag Berlin.

Budyko, M. I. 1958. The heat balance of the Earth's surface. English translation by U.S. Weather Bureau, Washington, D.C.

Budyko, M. I. 1963. Atlas of the heat balance of the Earth (in Russian). Kartfabrika Gosgeoltehizdata, Leningrad.

Bunker, A. 1976. Computations of surface energy flux and annual sea-air interaction cycles of the North Atlantic Ocean. *Mon. Weather Rev. 104,* 1122–1140.

Bunker, A. & Worthington, L. V. 1976. Energy exchange charts of the North Atlantic Ocean. *Bull. Amer. Meteorol. Soc. 57,* 670–678.

Cromwell, T. 1953. Circulation in a meridional plane in the Central Equatorial Pacific. *J. Mar. Res. 12,* 196–213.

Emery, W. J. 1976. The role of vertical motion in the heat budget of the upper Northeastern Pacific Ocean. *J. Phys. Oceanogr. 6,* 299–305.

Flohn, H. 1972. *Investigations of equatorial upwelling and its climatic role.* Studies of Physical Oceanography, tribute to Georg Wüst on his 80th birthday, Ed. A. C. Gordon, New York and London: Gordon and Breach, *1,* 93–102.

Hastenrath, S. & Lamb, P. 1977. *Climatic atlas of the tropical Atlantic and Eastern Pacific Oceans.* University of Wisconsin Press.

Yoshida, K. & Mao, H. L. 1957. A theory of upwelling of large horizontal extent. *J. Mar. Res. 16,* 40–54.

ПОЛУСФЕРНАЯ АСИММЕТРИЯ БЮДЖЕТА ТЕПЛА В ОКЕАНЕ В ЭКВАТОРИАЛЬНОЙ АТЛАНТИКЕ И В ВОСТОЧНОЙ ЧАСТИ ТИХОГО ОКЕАНА

Бюджет тепла в океане изучается на основе корабельных наблюдений за 1911–70 гг., собранных по площадям в 1 квадратный градус. Вращающийся по часовой стрелке поток воздуха вблизи поверхности через экватор способствует опусканию вод к югу и поднятию к северу от экватора в Атлантике и в восточной части Тихого океана, особенно, во время лета в северном полушарии. Вызываемое ветром поле вертикальных движений рассматривается как фактор поддержания языков холодной воды непосредственно к югу от экватора и сильного увеличения температуры к северу через экватор. Результирующая радиация лишь слегка выше в экваториальной зоне южного полушария, но потоки ощутимого и скрытого тепла сильно уменьшены в областях холодной воды, особенно летом в северном полушарии. В результате океан экспортирует тепло со скоростью 53 и 62 Вт/м^2 к югу от экватора в Атлантике и в Тихом океане, соответственно, по сравнению с экспортом в 29 и импортом в 3 Вт/м^2 в экваториальной зоне северного полушария.